Probing Zn^{2+}-binding effects on the zinc-ribbon domain of human general transcription factor TFIIB

Mahua GHOSH*, Laura M. ELSBY†, Tapas K. MAL*, Jane M. GOODING*, Stefan G. E. ROBERTS† and Mitsuhiko IKURA*[1]

*Division of Molecular and Structural Biology, Ontario Cancer Institute and Department of Medical Biophysics, University of Toronto, Toronto, Ontario M5G 2M9, Canada, and †School of Biological Sciences, G. 186 Stopford Building, University of Manchester, Oxford Road, Manchester M13 9PT, U.K.

The general transcription factor, TFIIB, plays an important role in the assembly of the pre-initiation complex. The N-terminal domain (NTD) of TFIIB contains a zinc-ribbon motif, which is responsible for the recruitment of RNA polymerase II and TFIIF to the core promoter region. Although zinc-ribbon motif structures of eukaryotic and archaeal TFIIBs have been reported previously, the structural role of Zn^{2+} binding to TFIIB remains to be determined. In the present paper, we report NMR and biochemical studies of human TFIIB NTD, which characterize the structure and dynamics of the TFIIB Zn^{2+}-binding domain in both Zn^{2+}-bound and -free states. The NMR data show that, whereas the backbone fold of NTD is pre-formed in the apo state, Zn^{2+} binding reduces backbone mobility in the β-turn (Arg^{28}–Gly^{30}), induces enhanced structural rigidity of the charged-cluster domain in the central linker region of TFIIB and appends a positive surface charge within the Zn^{2+}-binding site. V8 protease-sensitivity assays of full-length TFIIB support the Zn^{2+}-dependent structural changes. These structural effects of Zn^{2+} binding on TFIIB may have a critical role in interactions with its binding partners, such as the Rpb1 subunit of RNA polymerase II.

Key words: dynamics, general transcription factor, NMR, TFIIB, zinc ribbon.

INTRODUCTION

Efficient initiation of DNA template transcription requires the assembly of RNA polymerase II (pol II) and a set of general transcription factors. These general transcription factors are TFIIA, TFIIB, TFIID [including the promoter binding subunit of TFIID, the TATA-binding protein (TBP)], TFIIE, TFIIF and TFIIH [1–3]. These general transcription factors and pol II assemble on a class II promoter to form the functional pre-initiation complex (PIC) [2]. At the initial stage of this PIC assembly [1,2], TFIIB binds to the TBP (TFIID)–DNA complex and acts as a molecular bridge to pol II and the remaining general transcription factors [4].

Human TFIIB (hIIB, 316 amino acid residues) consists of two domains: the N-terminal domain (NTD; residues Met^1–Ala^{60}) and the C-terminal domain (CTD; residues Arg^{112}–Leu^{316}). The structure of hIIB CTD has been determined both in isolation [5] and in complex with promoter-bound TBP [6]. The NTD, being highly conserved from yeast to human, contains a zinc-ribbon motif [7], which interacts with TFIIF and guides pol II into the PIC [8]. The NTD also plays a crucial role in selecting the transcription-initiation site [9,10]. The zinc-ribbon motif with a Cys-Xaa_2-His-Xaa_{15}-Cys-Xaa_2-Cys sequence [11] contains a rubredoxin knuckle [12]. This motif can also bind Fe^{2+} and Co^{2+}, in a manner consistent with Fe^{2+} binding to rubredoxin. Although other zinc-ribbon or -finger structures consist of two Cys-Xaa-Xaa-His/Cys rubredoxin knuckles, the TFIIB zinc ribbon comprises one such knuckle at the C-terminal Cys-Xaa-Xaa-Cys region and a type I turn at the N-terminal Cys-Xaa-Xaa-His region [13]. This zinc-ribbon motif with a $\beta\beta\beta$ topology is highly conserved among eukaryotic and archaeal TFIIBs and can be found in other transcription factors, such as TFIIS [14,15], pol II subunits [14,16,17] and TFIIE [18,19].

In several transcription factors that contain the Zn^{2+}-finger motifs, Zn^{2+} plays an important role in maintaining the structural integrity required for functioning, i.e. sequence-specific DNA recognition [20]. To date, the role of Zn^{2+} binding to the TFIIB zinc-ribbon motif is not, however, well defined. In the present study, we calculated the structures of Zn^{2+}-bound and -free hIIB NTD by the use of ^1H–^{15}N residual dipolar couplings (RDCs) [21,22] in combination with the previously reported distance restraints deduced from nuclear Overhauser enhancement (NOE) analysis [13]. Furthermore, we have characterized the change in backbone dynamics that results from the depletion of Zn^{2+} around the Zn^{2+}-binding site through the use of backbone heteronuclear $\{^1H\}$–^{15}N NOE. These data correlate with the presented V8 protease-sensitivity experiments, as well as previous mutagenesis data [9].

EXPERIMENTAL

Overexpression and purification of hIIB NTD

The pETIIb plasmid, containing the gene encoding the hIIB NTD (Met^1–Ala^{60}), was transformed into the *Escherichia coli* strain BL21(DE3) (Novagen) [7]. Protein was overexpressed in Luria–Bertani both at 37 °C and purified in essentially the same manner as previously described [7]. Uniformly ^{15}N-labelled protein was obtained by using $^{15}NH_4Cl$ as the sole nitrogen source in M9 medium containing 50 μM $ZnCl_2$.

Abbreviations used: CCD, charged-cluster domain; CTD, C-terminal domain; 2D, two-dimensional; hIIB, human general transcription factor IIB; HSQC, heteronuclear single quantum coherence; IPAP, in-phase/anti-phase; NOE, nuclear Overhauser effect; NTD, N-terminal domain; PIC, pre-initiation complex; pol II, polymerase II; RDC, residual dipolar coupling; RMSD, root mean square deviation; TBP, TATA-binding protein; TFIIB, general transcription factor IIB.

[1] To whom correspondence should be addressed (e-mail mikura@uhnres.utoronto.ca).

The atomic co-ordinates and structural restraint data have been submitted to the RCSB (Research Collaboratory for Structural Bioinformatics) Protein Data Bank under the accession codes 1RO4 for apo-hIIB NTD and 1RLY for Zn^{2+}-bound hIIB NTD.

The NMR samples of ^{15}N-labelled Zn^{2+}-free and -bound hIIB NTD comprised 500 μl of 0.6 mM protein in $H_2O/^2H_2O$ (19:1, v/v) which contained 20 mM [$^2H_4$]imidazole hydrochloride (C/D/N Isotopes, Pointe Claire, Québec, Canada), 2.5 mM $ZnCl_2$, 5 % (v/v) glycerol and 20 mM sodium sulphate at pH 6.5. Zn^{2+}-free ^{15}N-labelled hIIB NTD protein samples were prepared by extensive dialysis against a buffer containing the chelating agent, Chelex-100 [23]. The NMR spectra of this sample were essentially identical with those recorded in the presence of Chelex-100 or 10 mM citric acid, a Zn^{2+}-chelator used for TFIIB [24]. Moreover, the addition of an excess of Zn^{2+} to these metal-bleached samples reproduced the Zn^{2+}-bound spectra. Partial alignment in the isotropic Zn^{2+}-bound and -free hIIB NTD sample was obtained by adding 12 mg/ml filamentous phage, Pf1 (ASLA Biotech, Riga, Latvia).

NMR spectroscopy

NMR spectra were acquired at 25 °C on a Varian INOVA 600 MHz spectrometer equipped with a triple-resonance pulse-field gradient probe. ^{1}H–^{15}N heteronuclear single quantum coherence (HSQC) spectra were recorded with 128 and 512 complex points in t_1 and t_2 respectively. ^{1}H–^{15}N RDCs were recorded using a two-dimensional (2D) IPAP (in-phase/anti-phase)-type sensitivity-enhanced ^{1}H–^{15}N HSQC correlation experiment [25]. The IPAP strategy records $^1J_{NH}$ separated doublets that are either in phase (IP) or anti-phase (AP). These data were then combined to give spectra containing only up-field or down-field components [26]. All 2D IPAP experiments were carried out with 256 and 512 complex points in t_1 and t_2 respectively. The final data set comprised 1024 and 4096 real points with a digital resolution of 2 and 2.2 Hz/point in F_1 and F_2 respectively. ^{1}H–^{15}N RDCs for both the Zn^{2+}-bound and -free states were determined by subtracting the splitting value obtained from each sample with and without alignment medium. Steady-state 2D $\{^1H\}$–^{15}N NOE spectra were acquired using the previously described method [27]. The heteronuclear NOE effect was calculated as the ratio of resonance intensities in the spectra with and without proton saturation. Spectra recorded with proton saturation utilized a 7 s recycle delay followed by a 5 s period of saturation using a train of ^{1}H 120° pulses every 5 ms. Spectra recorded in the absence of saturation employed a recycle delay of 12 s. NMR data sets were processed and analysed using NMRPipe [28], NMRDraw [28], and NMRView [29].

The chemical-shift changes between the two spectra of Zn^{2+}-bound and -free hIIB NTD were defined as the normalized weighted mean differences (Δ_{av}/Δ_{max}) for ^{1}H and ^{15}N [30]. This Δ_{av}(NH) is defined as $\{[\Delta H^2 + (\Delta N/5)^2]/2\}^{1/2}$, where ΔH and ΔN are the chemical shift changes between the Zn^{2+}-bound and -free states.

The structures of Zn^{2+}-bound and -free hIIB NTD were calculated using a simulated annealing protocol within the program CNS [31]. This calculation included both ^{1}H–^{15}N RDCs and NOE restraints. The distance restraint set was generated from the previously reported solution structure of hIIB NTD (Protein Data Bank code 1DL6) using MOLMOL [32] with a cut-off value of 5 Å. The calculations performed to determine the present structure employed the same number of distance restraints as used in the determination of the previous NMR structure [13]. In the case of the Zn^{2+}-bound state, covalent restraints of the (Cys_3His) Zn^{2+} centre were incorporated into the structure calculation, as previously described [13]. These structural statistics are shown in Table 1. The atomic co-ordinates and structural restraint data have been submitted to the RCSB (Research Collaboratory for Structural Bioinformatics) Protein Data Bank under the accession codes 1RO4 for apo-hIIB NTD and 1RLY for Zn^{2+}-bound hIIB NTD.

Table 1 Experimental restraints and structural statistics for the lowest-energy structures of hIIB NTD

	Zn^{2+}-free	Zn^{2+}-bound
Calculated structures		
⟨SA⟩*	30	25
Experimental restraints		
Distance restraints†	443	443
Zn^{2+} co-ordination restraints†	–	10
^{1}H–^{15}N RDC restraints	22	23
Structural statistics		
RDC violations	0	0
RMSD from ideal geometry		
Bonds	0.0026 ± 0.00003	0.0037 ± 0.00006
Angles	0.484 ± 0.008	0.597 ± 0.004
Impropers	0.306 ± 0.021	0.428 ± 0.031
Residues in the allowed region of Ramachandran plot (%)	95	94.8
RMSD (all backbone atoms)‡	0.36 ± 0.11	0.51 ± 0.11
RMSD (all heavy atoms)‡	0.76 ± 0.11	1.00 ± 0.16

* ⟨SA⟩ is the ensemble of NMR-derived simulated annealing structures.

† Distance restraints were calculated from the previous structure (Protein Data Bank code 1DL6) using MOLMOL [32]. The distance restraints used were equal in number as in the solution NMR structure.

‡ The ensemble was superimposed on N, C′, C^α atoms of residues in the well-defined region (residues 14–26 and 31–42) of hIIB NTD.

V8 protease assay

Recombinant TFIIB and its derivatives, containing a C-terminal T7 epitope tag, were prepared as described previously [8]. TFIIB was subjected to site-directed mutagenesis using the QuickChange kit (Stratagene). Partial digestion with V8 protease was performed as previously described [33], and the products resolved by electrophoresis were detected using anti-T7 monoclonal antibody (Novagen). To produce the apo-TFIIB derivatives, recombinant TFIIBs (or mutants) were dialysed into 10 mM citric acid buffer as described previously [24] and then into buffer containing 20 % (v/v) glycerol, 20 mM Hepes, 100 mM KCl, 0.2 mM EDTA, 1 mM dithiothreitol at pH 8. Where indicated, $ZnCl_2$ was added back to apo-TFIIB at a concentration of 1 μM.

RESULTS

Zn^{2+}-free hIIB NTD retains the zinc-ribbon-motif fold

To probe effects of Zn^{2+} binding on the conformation of TFIIB, we recorded ^{1}H–^{15}N correlated HSQC spectra of ^{15}N-labelled hIIB NTD in both Zn^{2+}-bound and -free states (Figure 1b). We found that the ^{1}H and ^{15}N chemical shifts of a number of residues in hIIB NTD were perturbed upon addition of Zn^{2+}. The most noticeable change was observed in the Zn^{2+}-co-ordinating residues, Cys^{15} and Cys^{37} (0.09 and 0.08 p.p.m. respectively for ^{1}H, 0.24 and 0.08 p.p.m. respectively for ^{15}N). Several acidic and hydrophobic residues were also perturbed, with an average shift of 0.028 p.p.m. (^{1}H) and 0.28 p.p.m. (^{15}N), including residues Asp^{20}, Asp^{31}, Glu^{36}, Ile^{22}, Leu^{23}, Met^{32} and Leu^{39}. Among the other perturbed residues, Leu^{23}, Met^{32}, Leu^{39} and Gly^{42} are located in the conserved β-sheet region; Arg^{28}, Ala^{29} and Gly^{30} in the loop region; and Ala^{21} and Tyr^{27} before the β strands (Figure 1a).

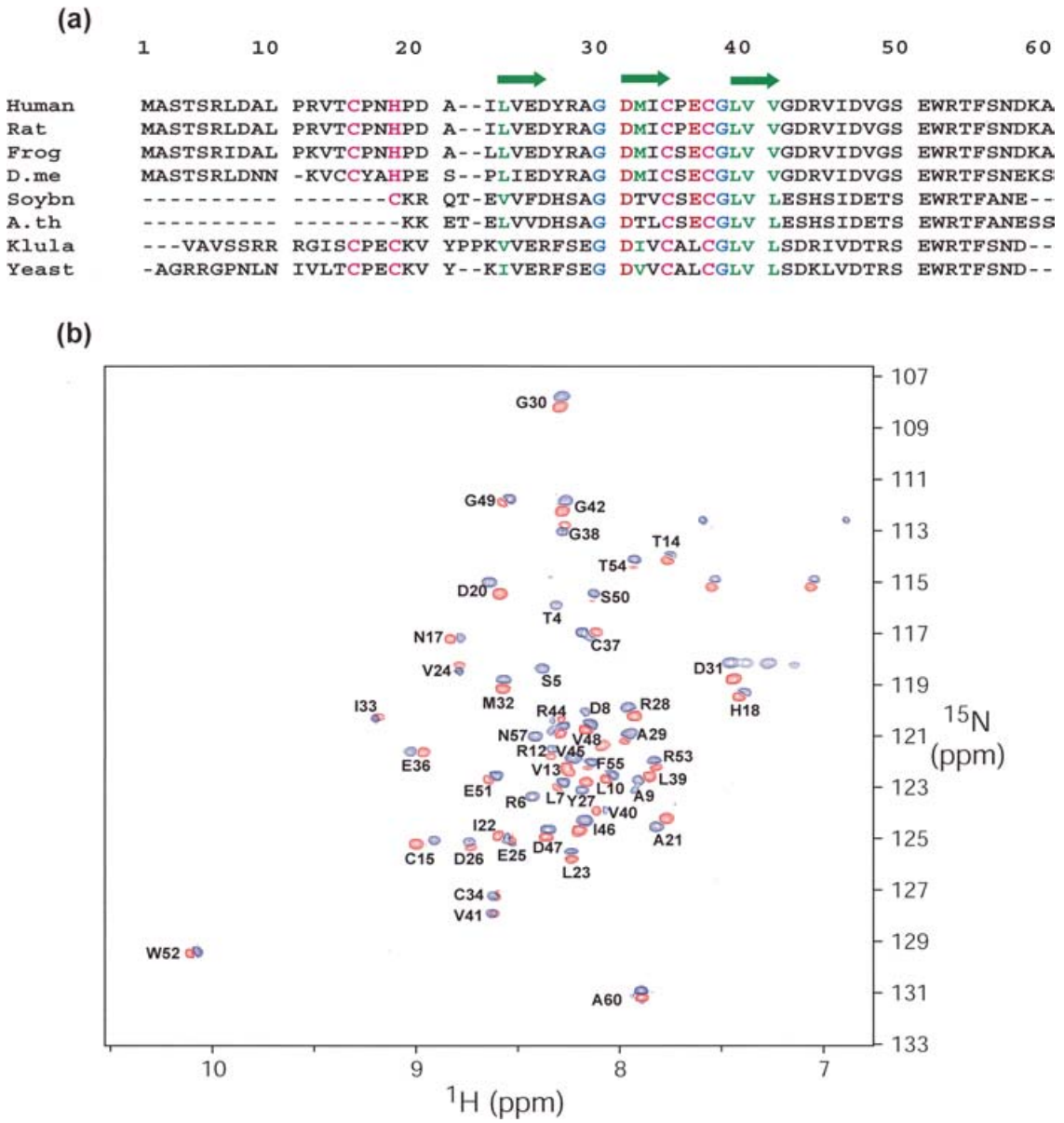

Figure 1 (a) Sequence alignment of zinc-ribbon motifs from various organisms and (b) ^{1}H–^{15}N HSQC spectra of hIIB NTD

(**a**) Sequence alignment of zinc-ribbon motifs found in TFIIBs from various organisms. The conserved amino acids are colour coded: magenta represents the Zn^{2+} co-ordinating residues, green represents the hydrophobic residues, red represents the acidic residues and glycine residues are in blue. D. me, *Drosophila melanogaster*; Soybn, soybean; A. th, *Arabidopsis thaliana*; Klula, *Kluyveromyces lactis*. (**b**) ^{1}H–^{15}N HSQC spectra of the Zn^{2+}-free (red) and -bound (blue) states of hIIB NTD.

In recent years, RDCs have been successfully used in refinement of protein structures determined by the conventional NOE-driven method [34,35]. In the present study, we measured ^{1}H–^{15}N RDCs from the Zn^{2+}-bound hIIB NTD sample, which were used to refine the previously reported structure of the Zn^{2+}-bound hIIB NTD [13]. The additional RDC-derived constraints produced no major violations in structure calculation, and the resulting overall structure of hIIB NTD is similar to that previously determined. However, the use of RDCs in combination with the distance restraints improved the precision of the structural region of hIIB NTD (Thr^{14}–Gly^{42}) when compared with the previous structure. The average pairwise backbone RMSD (root mean square deviation) for the refined structure is 0.51 Å (1 Å = 0.1 nm), compared with 0.74 Å for the previously determined structure of the Zn^{2+}-bound hIIB NTD.

Bax and co-workers [36] demonstrated previously for calmodulin, a Ca^{2+}-binding protein, that a relatively small number of RDC-driven constraints are sufficient to derive the structure of the apo (Ca^{2+}-free) state starting from the Ca^{2+}-bound structure or vice versa. In light of the relatively small chemical-shift changes observed in ^{1}H–^{15}N HSQC, the lack of obvious differences in secondary-structure assignments using the chemical-shift index [37] and the absence of changes in short-range sequential NOEs between residues i and $i+1$, we used the previously reported structure of the Zn^{2+}-bound hIIB NTD [13] as an initial model to calculate the Zn^{2+}-free structure with ^{1}H–^{15}N RDC data measured

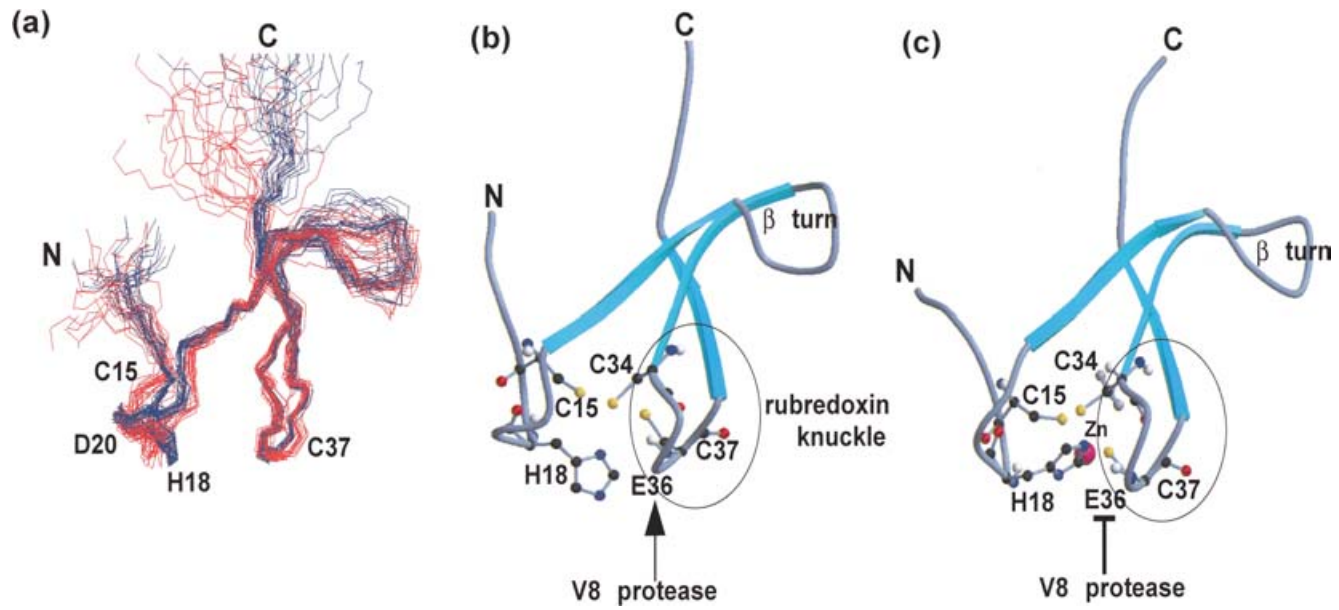

Figure 2 RDC-derived structural models of Zn^{2+}-free and -bound hIIB NTD

(**a**) Best-fit superimposition of the 30 and 25 solution structures of Zn^{2+}-free (red) and Zn^{2+}-bound (blue) hIIB NTD respectively. Only the backbone C′, C^{α} and N atoms in the well-defined regions of the protein (residues 14–26 and 31–42) are superimposed. This Figure was generated using MOLMOL [32]. (**b**) and (**c**) Ribbon representation, of Zn^{2+}-free and -bound hIIB NTD respectively. These Figures were generated using MOLSCRIPT [48].

experimentally from the Zn^{2+}-free hIIB NTD sample. With a total of 22 ^{1}H–^{15}N RDC restraints, 30 of the lowest-energy structures were generated in the Zn^{2+}-free (Figure 2a) state, and the average pairwise backbone RMSDs for these structures is 0.36 Å.

Comparison between Zn^{2+}-bound and -free hIIB NTD structures provides insights into Zn^{2+}-dependent conformational changes within this domain. Not surprisingly, the overall backbone fold of the Zn^{2+}-free state is essentially identical with that of the Zn^{2+}-bound state. However, we noticed some backbone conformational changes near the Zn^{2+}-binding site. These localized changes involve the backbone conformation of the type I turn at one face of the Zn^{2+}-binding site, comprising Cys^{15}–His^{18}, which is coupled with a smaller change in the rubredoxin knuckle at the opposite face of the Zn^{2+}-binding site, containing Glu^{36}, Cys^{37}, Gly^{38} and Leu^{39} (Figure 2). Five of the six rubredoxin-knuckle-constituting residues (Cys^{34}, Glu^{36}, Cys^{37}, Gly^{38} and Leu^{39}) are highly conserved from yeast to humans (Figure 1a), suggesting similar, if not identical, structural elements and Zn^{2+}-binding properties among eukaryotic TFIIBs. Interestingly, previous mutagenesis studies on yeast TFIIB (yIIB) have identified Leu^{50} (equivalent to Leu^{39} in hIIB) as the critical residue for pol II binding [9]. Furthermore, the mutation $Gly^{49} \rightarrow Ser$ (equivalent to Gly^{38} in hIIB) produces a cold-sensitive phenotype [38]. These mutational data indicate the importance of the structural integrity around the Zn^{2+}-binding site for the IIB function.

Zn^{2+}-dependent change in backbone dynamics

In order to gain insight into the backbone mobility of the hIIB NTD upon Zn^{2+} depletion, the steady-state $\{^{1}H\}$–^{15}N NOEs for both Zn^{2+}-bound and -free states were measured. In particular, we attempted to characterize the flexibility of the β-turn region comprising residues Arg^{28}–Gly^{30}, for which the backbone atom positions are not well defined (Figure 2). The NOE values indicate that the overall profile of backbone mobility in the structured region (Thr^{14}–Gly^{42}) is very similar between the Zn^{2+}-bound and -free states (Figure 3b). Interestingly, for both states, the NOE profile drops slightly in the central β-turn region (Arg^{28}–Gly^{30}), suggesting a higher mobility relative to the rest of the structured region. Moreover, Ala^{29} in the Zn^{2+}-free state shows a drastically reduced NOE value (Figure 3d). As this β-turn region possesses a higher flexibility than the corresponding region in the Zn^{2+}-bound state, it was not included in the distance constraints used during the aforementioned structure calculation.

The steady-state $\{^{1}H\}$–^{15}N NOE data show further that the NOE values of two separate regions just outside the zinc-ribbon motif fold (Thr^{4}–Arg^{12} and Asp^{43}–Phe^{55}) are significantly higher in the Zn^{2+}-bound state. The latter region, which undergoes Zn^{2+}-induced structural rigidity, may have a structural/functional role, as it coincides with the charged-cluster domain (CCD) in the TFIIB linker region [39], a region known to be crucial for maintaining the proper intramolecular interaction between NTD and CTD [40].

Enhanced proteolytic sensitivity of hIIB NTD

It has been shown that proteolysis using V8 protease is sensitive to changes in the conformation of TFIIB [33,41]. Accordingly, we employed this assay to determine whether Zn^{2+} binding can change this V8 protease sensitivity. A previously described TFIIB derivative, tagged at the C-terminus with a 10-amino-acid T7 epitope detected in Western blotting by a monoclonal antibody [33], was used in the present study. We observed that wild-type TFIIB is relatively stable against proteolysis by the V8 protease (Figure 4a). However, when TFIIB is dialysed into citric acid to remove the Zn^{2+} (apo-IIB), the N-terminus of TFIIB becomes sensitive to V8 protease cleavage, producing a single major fragment detected by anti-T7 antibody (represented by an asterisk in Figure 4). The size difference indicates that a segment

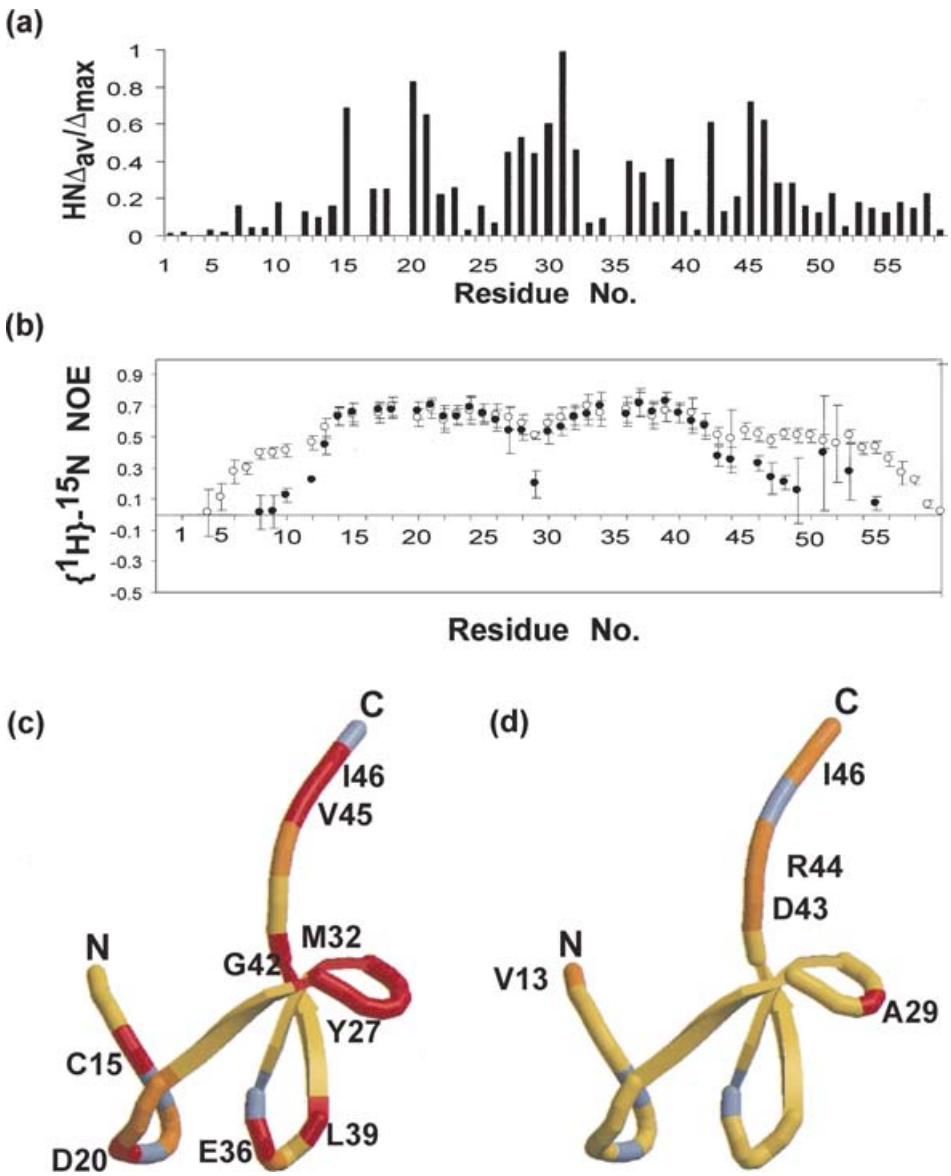

Figure 3 Effect of Zn^{2+} binding on chemical shifts and $\{^1H\}$–^{15}N NOE

(**a**) The normalized weighted mean chemical-shift differences (Δ_{av}/Δ_{max}) following Zn^{2+} binding to hIIB NTD for ^1H and ^{15}N plotted as a function of the residues. (**b**) Plot of steady-state $\{^1H\}$–^{15}N NOE data of the Zn^{2+}-free (●) and -bound (○) states of hIIB NTD as a function of the residues. Errors in the NOE values were estimated from the signal-to-noise ratio of each spectrum. (**c**) The effects of Zn^{2+} binding on the chemical shift changes are mapped on the Zn^{2+}-bound hIIB NTD structure. The extent of the chemical-shift changes is represented in the following colour code: yellow (Δ_{av}/Δ_{max}) > 0.1 p.p.m. to red (Δ_{av}/Δ_{max}) $\geqslant$ 0.4 p.p.m. and grey (Δ_{av}/Δ_{max}) $\leqslant$ 0.01 p.p.m. The Figure was generated using MOLSCRIPT [48]. (**d**) The differences in NOE values between Zn^{2+}-free and -bound states are mapped on the Zn^{2+}-bound structure. Red, orange and yellow represent large, medium and small changes respectively. The residues for which no data were available are represented in grey. The Figure was generated using MOLSCRIPT [48].

of approx. 30–50 amino acids is cleaved from the N-terminus of TFIIB. Addition of Zn^{2+} to the Zn^{2+}-free TFIIB sample recovers protease resistance at this N-terminal V8 protease-cleavage site. Thus removal of Zn^{2+} from TFIIB induces an alteration in the conformation of the N-terminus of TFIIB.

We also carried out the V8 protease assay on the TFIIB mutant $Cys^{34} \rightarrow Ala$. Consistent with the removal of Zn^{2+} from TFIIB by dialysis, the $Cys^{34} \rightarrow Ala$ mutant produces a fragment of slightly smaller size than that of the wild-type TFIIB (Figure 4b). Thus the $Cys^{34} \rightarrow Ala$ mutation causes a conformational change somewhat similar to the change induced by the removal of Zn^{2+} from the NTD. Among the two possible sites for V8 cleavage in the NTD region (Glu^{25} and Glu^{36}), our calculated structures for both Zn^{2+}-free and -bound states indicates that Cys^{34} is in close proximity to Glu^{36}, but not to Glu^{25}. Indeed, the results shown in Figure 4(c) demonstrate that only the $Glu^{36} \rightarrow Ala$ mutation abolishes this Zn^{2+}-dependent V8 protease sensitivity.

DISCUSSION

The RDC-based NMR structure determination enabled us to probe conformational changes in hIIB NTD induced by Zn^{2+} binding. An observed change in backbone conformation is localized in the

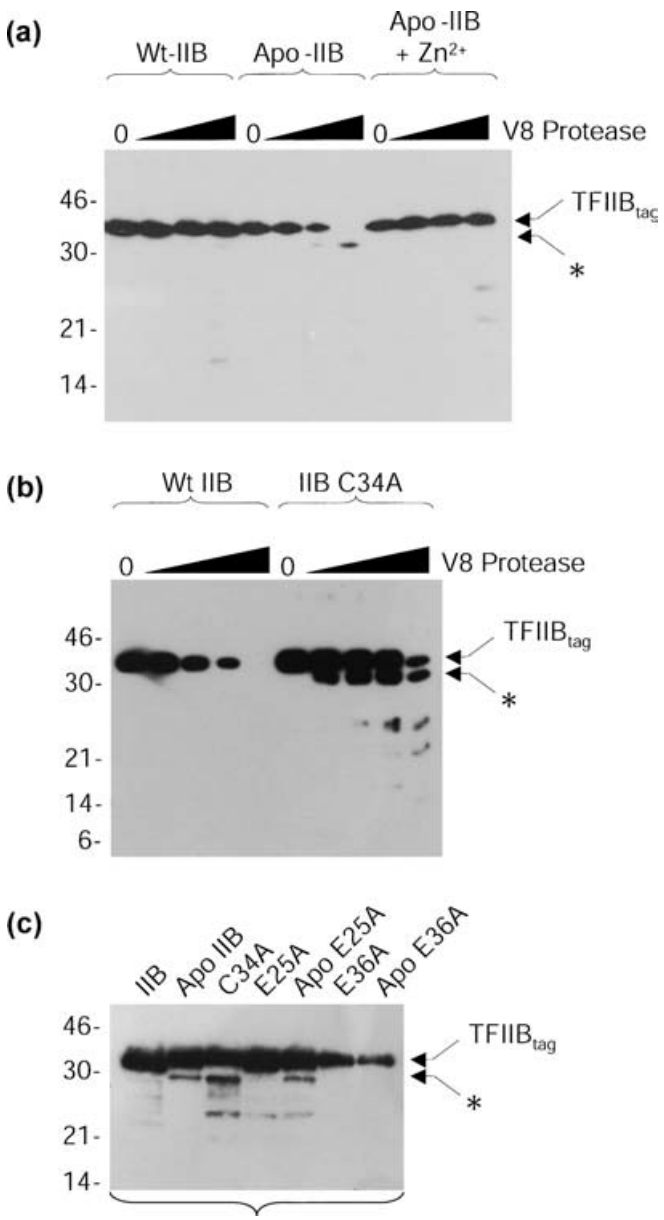

Figure 4 V8 protease sensitivity of hIIB

(**a**) Western blot showing the V8 protease-cleavage pattern of the TFIIB epitope tagged at the C-terminus in wild-type (Wt) TFIIB, Zn^{2+}-free TFIIB and Zn^{2+}-bound TFIIB. Each set of lanes contains 40 ng of TFIIB treated with 0, 0.02, 0.1 or 0.5 ng of V8 protease. (**b**) Western blot of wild-type and a $Cys^{34} \rightarrow Ala$ (C34A) mutant of TFIIB (40 ng each) after addition of V8 protease (0, 0.1, 0.5, 2 or 10 ng). (**c**) Western blot of wild-type TFIIB (40 ng) and the indicated derivatives [$Cys^{34} \rightarrow Ala$ (C34A), $Glu^{25} \rightarrow Ala$ (E25A) and $Glu^{36} \rightarrow Ala$ (E36A); either native or dialysed to remove Zn^{2+} (designated Apo)] cleaved with V8 protease (0.5 ng). Molecular-mass markers (kDa) are indicated on the left.

region that constitutes the Zn^{2+}-binding site, which consists of the N-terminal type I turn (Cys^{15}–Leu^{23}), the β-turn (Arg^{28}–Gly^{30}) and the rubredoxin knuckle (Cys^{34}–Gly^{38}). Whereas the backbone conformation of the N-terminal type I turn and the rubredoxin knuckle rearranges itself, the mobility of these segments is not largely affected by the absence of Zn^{2+}, as evidenced by steady-state $\{^1H\}$–^{15}N NOE measurements. It is only the central β-turn (Arg^{28}–Gly^{30}) that experiences a higher mobility in the Zn^{2+}-free state.

The Zn^{2+}-dependent conformational changes in hIIB NTD are in agreement with the V8 protease-sensitivity assay experiments. We found that the depletion of Zn^{2+} results in a specific proteolytic cleavage at Glu^{36}, a residue located in the rubredoxin knuckle. Enhanced protease sensitivity is most likely to be coupled to a localized conformational rearrangement within the Zn^{2+}-binding site described above. Although the fold of the zinc-ribbon motif is maintained in the Zn^{2+}-free state of TFIIB, the removal of Zn^{2+} from the binding site induces a subtle, but significant, backbone and side-chain conformational rearrangement, which in turn influences the V8 protease sensitivity in this region.

Previous limited V8 protease experiments [33] revealed that the herpes simplex virus transcription activator VP16 induces an enhanced V8 sensitivity of Glu^{51} in the CCD, a region critical for maintaining the intramolecular interaction between the NTD and CTD [39]. This involves a global alternation in the NTD–CTD interaction and spatial orientation, represented by the closed-to-open conformational change and the reversible interaction between the NTD and CTD [33]. The V8 sensitivity of Glu^{51} is completely abolished in VP16-free TFIIB, which is presumably bound with Zn^{2+} under the conditions used. Our steady-state $\{^1H\}$–^{15}N NOE data suggest that Zn^{2+} binding contributes to the rigidification of the CCD at the TFIIB domain linker. This long-range effect on Zn^{2+} binding, which is also supported by Zn^{2+}-dependent chemical-shift changes (Figure 3a), may have a role in the intramolecular interaction of TFIIB. Interestingly, a structural cross-talk between the zinc-ribbon domain and the CCD is suggested by a recent study, which showed that the $Glu^{51} \rightarrow$ Arg mutation in the CCD perturbs the transcription start site [40].

Recent crystallographic studies on the yeast pol II multi-subunit complex have dramatically advanced our understanding of the structure of the transcription initiation machinery [42–44]. Although TFIIB was not included in those structures, Kornberg and co-workers [42,43] suggested that TFIIB might bind to the 'Dock' domain of Rpb1. More recently, site-specific photocross-linking and directed hydroxyl radical probing studies by Chen and Hahn [45] showed that the zinc-ribbon domain of TFIIB is responsible for the proposed interaction with the Rpb1 Dock domain. Our comparison of the electrostatic potential of the molecular surface between Zn^{2+}-bound and -free states (Figure 5) shows a positively charged cluster in the Zn^{2+}-bound state, with no other significant change in the electrostatic or hydrophobic character of the molecular surface. Interestingly, an acidic region, which includes the adjacent 'Linker' domain in Rpb1, has been suggested to interact with TFIIB [46]. It is tempting to speculate that the Zn^{2+}-induced positively charged surface may interact with this acidic region in Rpb1. In addition, there is a highly conserved cluster of hydrophobic residues on the surface of the TFIIB zinc-ribbon domain (Figure 1), which consists of Met^{32}, Ile^{33}, Leu^{39} and Val^{40} in human TFIIB. Together with the potential electrostatic interactions described above, these residues may participate in the interaction with pol II and/or TFIIF [47].

In summary, the observed Zn^{2+}-dependent conformational change in the hIIB NTD is restricted to small areas of the zinc-ribbon motif. Our NMR-based dynamics study indicates that Zn^{2+} binding induces a long-range effect on the mobility of the CCD region outside of the zinc-ribbon motif. As the CCD region plays a critical role in the TFIIB function [39], Zn^{2+} binding may also contribute to this biological function via stabilization of the CCD structure. Further studies are needed to elucidate how Zn^{2+} binding to NTD could propagate its effect to the structural integrity of the whole TFIIB molecule, which in turn determines its ability to facilitate PIC assembly, start-site selection and transcriptional activation.

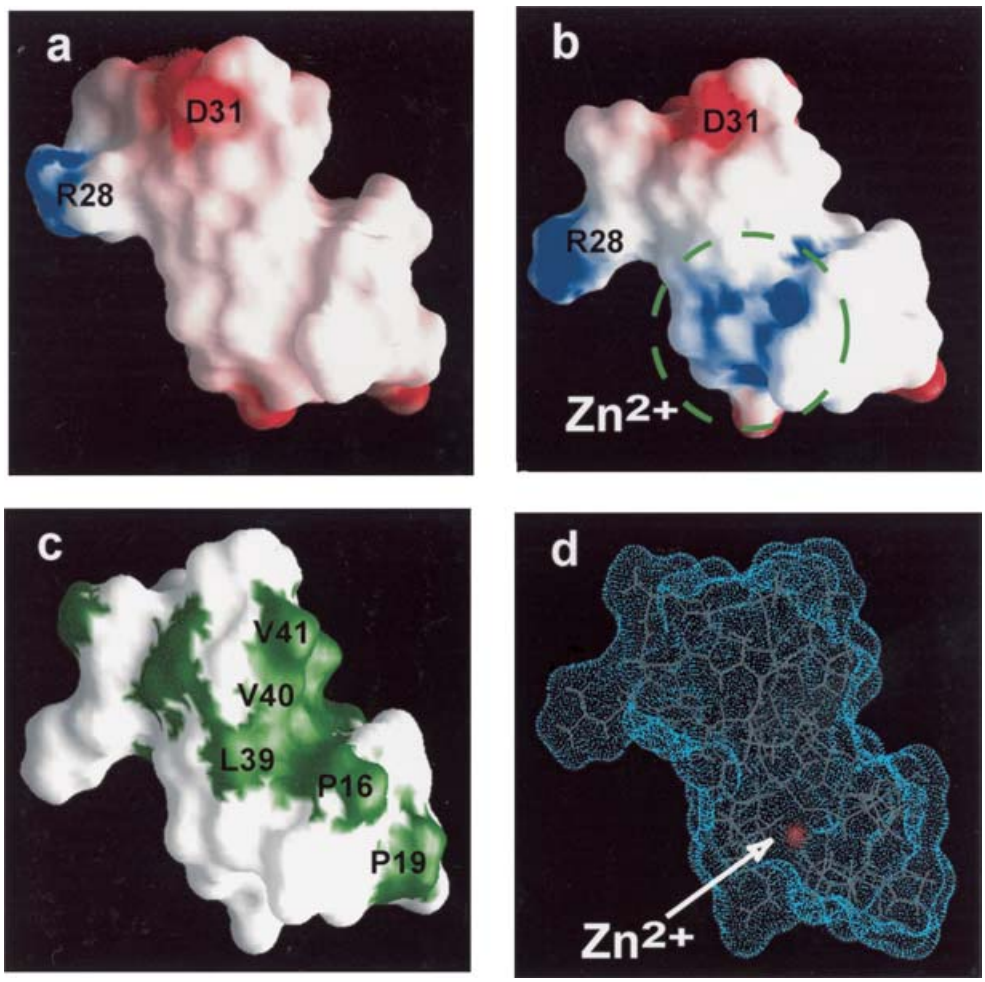

Figure 5 Molecular surface representation of hIIB NTD

(**a**) and (**b**) Electrostatic potential maps of hIIB NTD, where red and blue represent negative and positive potentials respectively. The green broken circle in (**b**) represents a positively charged surface at the Zn^{2+}-binding site. (**c**) The hydrophobic patch mapped on the surface of hIIB NTD and (**d**) Zn^{2+} (shown as a red ball) located below the surface (dotted surface as plotted) of the molecule. The molecular surfaces were generated using GRASP [49].

We thank Danny Reinberg for providing us with the human TFIIB cDNA, Kit Tong for technical assistance, and Tadashi Nemoto for his involvement at the initial stage of this study. This work was supported by a grant from Canadian Institutes of Health Research (CIHR). L. M. E. is funded by a Wellcome Prize Studentship and S. G. E. R. by a Wellcome Trust Senior Fellowship. M. G. was supported by a CIHR fellowship and M. I. is a CIHR Senior Investigator.

REFERENCES

1 Zawel, L. and Reinberg, D. (1995) Common themes in assembly and function of eukaryotic transcription complexes. Annu. Rev. Biochem. **64**, 533–561
2 Orphanides, G., Lagrange, T. and Reinberg, D. (1996) The general transcription factors of RNA polymerase II. Genes Dev. **10**, 2657–2683
3 Roeder, R. G. (1996) The role of general initiation factors in transcription by RNA polymerase II. Trends Biochem. Sci. **21**, 327–335
4 Buratowski, S., Hahn, S., Guarente, L. and Sharp, P. A. (1989) Five intermediate complexes in transcription initiation by RNA polymerase II. Cell **56**, 549–561
5 Bagby, S., Kim, S., Maldonado, E., Tong, K. I., Reinberg, D. and Ikura, M. (1995) Solution structure of the C-terminal core domain of human TFIIB: similarity to cyclin A and interaction with TATA-binding protein. Cell **82**, 857–867
6 Nikolov, D. B., Chen, H., Halay, E. D., Usheva, A. A., Hisatake, K., Lee, D. K., Roeder, R. G. and Burley, S. K. (1995) Crystal structure of a TFIIB–TBP–TATA-element ternary complex. Nature (London) **377**, 119–128
7 Hayashi, F., Ishima, R., Liu, D., Tong, K. I., Kim, S., Reinberg, D., Bagby, S. and Ikura, M. (1998) Human general transcription factor TFIIB: conformational variability and interaction with VP16 activation domain. Biochemistry **37**, 7941–7951
8 Ha, I., Roberts, S., Maldonado, E., Sun, X., Kim, L. U., Green, M. and Reinberg, D. (1993) Multiple functional domains of human transcription factor IIB: distinct interactions with two general transcription factors and RNA polymerase II. Genes Dev. **7**, 1021–1032
9 Pardee, T. S., Bangur, C. S. and Ponticelli, A. S. (1998) The N-terminal region of yeast TFIIB contains two adjacent functional domains involved in stable RNA polymerase II binding and transcription start site selection. J. Biol. Chem. **273**, 17859–17864
10 Zhang, D. Y., Carson, D. J. and Ma, J. (2002) The role of TFIIB–RNA polymerase II interaction in start site selection in yeast cells. Nucleic Acids Res. **30**, 3078–3085
11 Laity, J. H., Lee, B. M. and Wright, P. E. (2001) Zinc finger proteins: new insights into structural and functional diversity. Curr. Opin. Struct. Biol. **11**, 39–46
12 Schwabe, J. W. and Klug, A. (1994) Zinc mining for protein domains. Nat. Struct. Biol. **1**, 345–349
13 Chen, H. T., Legault, P., Glushka, J., Omichinski, J. G. and Scott, R. A. (2000) Structure of a (Cys_3His) zinc ribbon, a ubiquitous motif in archaeal and eucaryal transcription. Protein Sci. **9**, 1743–1752
14 Qian, X., Gozani, S. N., Yoon, H., Jeon, C. J., Agarwal, K. and Weiss, M. A. (1993) Novel zinc finger motif in the basal transcriptional machinery: three-dimensional NMR studies of the nucleic acid binding domain of transcriptional elongation factor TFIIS. Biochemistry **32**, 9944–9959
15 Olmsted, V. K., Awrey, D. E., Koth, C., Shan, X., Morin, P. E., Kazanis, S., Edwards, A. M. and Arrowsmith, C. H. (1998) Yeast transcript elongation factor (TFIIS), structure and function. I: NMR structural analysis of the minimal transcriptionally active region. J. Biol. Chem. **273**, 22589–22594
16 Wang, B., Jones, D. N., Kaine, B. P. and Weiss, M. A. (1998) High-resolution structure of an archaeal zinc ribbon defines a general architectural motif in eukaryotic RNA polymerases. Structure **6**, 555–569

17 Cramer, P., Bushnell, D. A., Fu, J., Gnatt, A. L., Maier-Davis, B., Thompson, N. E., Burgess, R. R., Edwards, A. M., David, P. R. and Kornberg, R. D. (2000) Architecture of RNA polymerase II and implications for the transcription mechanism. Science **288**, 640–649
18 Ohkuma, Y., Sumimoto, H., Hoffmann, A., Shimasaki, S., Horikoshi, M. and Roeder, R. G. (1991) Structural motifs and potential σ homologies in the large subunit of human general transcription factor TFIIE. Nature (London) **354**, 398–401
19 Peterson, M. G., Inostroza, J., Maxon, M. E., Flores, O., Admon, A., Reinberg, D. and Tjian, R. (1991) Structure and functional properties of human general transcription factor IIE. Nature (London) **354**, 369–373
20 Berg, J. M. (1990) Zinc finger domains: hypothesis and current knowledge. Annu. Rev. Biophys. Biophys. Chem. **19**, 405–421
21 Tjandra, N. and Bax, A. (1997) Direct measurement of distances and angles in biomolecules by NMR in a dilute liquid crystalline medium. Science **278**, 1111–1114
22 Tolman, J. R., Flanagan, J. M., Kennedy, M. A. and Prestegard, J. H. (1995) Nuclear magnetic dipole interactions in field-oriented proteins: information for structure determination in solution. Proc. Natl. Acad. Sci. U.S.A. **92**, 9279–9283
23 Vorherr, T., James, P., Krebs, J., Enyedi, A., McCormick, D. J., Penniston, J. T. and Carafoli, E. (1990) Interaction of calmodulin with the calmodulin binding domain of the plasma membrane Ca^{2+} pump. Biochemistry **29**, 355–365
24 Freedman, L. P., Luisi, B. F., Korszun, Z. R., Basavappa, R., Sigler, P. B. and Yamamoto, K. R. (1988) The function and structure of the metal coordination sites within the glucocorticoid receptor DNA binding domain. Nature (London) **334**, 543–546
25 Kay, L. E., Keifer, P. and Saarinen, T. (1992) Pure absorption gradient enhanced heteronuclear single quantum correlation spectroscopy with improved sensitivity. J. Am. Chem. Soc. **114**, 10663–10665
26 Ottiger, M., Delaglio, F. and Bax, A. (1998) Measurement of J and dipolar couplings from simplified two-dimensional NMR spectra. J. Magn. Reson. **131**, 373–378
27 Farrow, N. A., Muhandiram, R., Singer, A. U., Pascal, S. M., Kay, C. M., Gish, G., Shoelson, S. E., Pawson, T., Forman-Kay, J. D. and Kay, L. E. (1994) Backbone dynamics of a free and phosphopeptide-complexed Src homology 2 domain studied by ^{15}N NMR relaxation. Biochemistry **33**, 5984–6003
28 Delaglio, F., Grzesiek, S., Vuister, G. W., Zhu, G., Pfeifer, J. and Bax, A. (1995) NMRPipe: a multidimensional spectral processing system based on UNIX pipes. J. Biomol. NMR **6**, 277–293
29 Johnson, B. A. and Blevins, R. A. (1994) NMRView: A computer program for the visualization and analysis of NMR data. J. Biomol. NMR **4**, 603–614
30 Foster, M. P., Wuttke, D. S., Clemens, K. R., Jahnke, W., Radhakrishnan, I., Tennant, L., Reymond, M., Chung, J. and Wright, P. E. (1998) Chemical shift as a probe of molecular interfaces: NMR studies of DNA binding by the three amino-terminal zinc finger domains from transcription factor IIIA. J. Biomol. NMR **12**, 51–71
31 Brunger, A. T., Adams, P. D., Clore, G. M., DeLano, W. L., Gros, P., Grosse-Kunstleve, R. W., Jiang, J. S., Kuszewski, J., Nilges, M., Pannu, N. S. et al. (1998) Crystallography and NMR system: a new software suite for macromolecular structure determination. Acta Crystallogr. Sect. D Biol. Crystallogr. **54**, 905–921
32 Koradi, R., Billeter, M. and Wuthrich, K. (1996) MOLMOL: a program for display and analysis of macromolecular structures. J. Mol. Graphics **14**, 51–55, 29–32
33 Roberts, S. G. and Green, M. R. (1994) Activator-induced conformational change in general transcription factor TFIIB. Nature (London) **371**, 717–720
34 Bax, A., Kontaxis, G. and Tjandra, N. (2001) Dipolar couplings in macromolecular structure determination. Methods Enzymol. **339**, 127–174
35 Clore, G. M., Gronenborn, A. M. and Tjandra, N. (1998) Direct structure refinement against residual dipolar couplings in the presence of rhombicity of unknown magnitude. J. Magn. Reson. **131**, 159–162
36 Chou, J. J., Li, S. and Bax, A. (2000) Study of conformational rearrangement and refinement of structural homology models by the use of heteronuclear dipolar couplings. J. Biomol. NMR **18**, 217–227
37 Wishart, D. S., Sykes, B. D. and Richards, F. M. (1992) The chemical shift index: a fast and simple method for the assignment of protein secondary structure through NMR spectroscopy. Biochemistry **31**, 1647–1651
38 Knaus, R., Pollock, R. and Guarente, L. (1996) Yeast SUB1 is a suppressor of TFIIB mutations and has homology to the human co-activator PC4. EMBO J. **15**, 1933–1940
39 Hawkes, N. A., Evans, R. and Roberts, S. G. (2000) The conformation of the transcription factor TFIIB modulates the response to transcriptional activators *in vivo*. Curr. Biol. **10**, 273–276
40 Fairley, J. A., Evans, R., Hawkes, N. A. and Roberts, S. G. (2002) Core promoter-dependent TFIIB conformation and a role for TFIIB conformation in transcription start site selection. Mol. Cell. Biol. **22**, 6697–6705
41 Agostini, I., Navarro, J. M., Bouhamdan, M., Willetts, K., Rey, F., Spire, B., Vigne, R., Pomerantz, R. and Sire, J. (1999) The HIV-1 Vpr co-activator induces a conformational change in TFIIB. FEBS Lett. **450**, 235–239
42 Cramer, P., Bushnell, D. A. and Kornberg, R. D. (2001) Structural basis of transcription: RNA polymerase II at 2.8 angstrom resolution. Science **292**, 1863–1876
43 Gnatt, A. L., Cramer, P., Fu, J., Bushnell, D. A. and Kornberg, R. D. (2001) Structural basis of transcription: an RNA polymerase II elongation complex at 3.3 Å resolution. Science **292**, 1876–1882
44 Armache, K. J., Kettenberger, H. and Cramer, P. (2003) Architecture of initiation-competent 12-subunit RNA polymerase II. Proc. Natl. Acad. Sci. U.S.A. **100**, 6964–6968
45 Chen, H. T. and Hahn, S. (2003) Binding of TFIIB to RNA polymerase II: mapping the binding site for the TFIIB zinc ribbon domain within the preinitiation complex. Mol. Cell **12**, 437–447
46 Xiao, H., Friesen, J. D. and Lis, J. T. (1994) A highly conserved domain of RNA polymerase II shares a functional element with acidic activation domains of upstream transcription factors. Mol. Cell. Biol. **14**, 7507–7516
47 Hahn, S. and Roberts, S. (2000) The zinc ribbon domains of the general transcription factors TFIIB and Brf: conserved functional surfaces but different roles in transcription initiation. Genes Dev. **14**, 719–730
48 Kraulis, P. J. (1991) MOLSCRIPT: a program to produce both detailed and schematic plots of protein structures. J. Appl. Crystallogr. **24**, 946–950
49 Nicholls, A., Sharp, K. A. and Honig, B. (1991) Protein folding and association: insights from the interfacial and thermodynamic properties of hydrocarbons. Proteins **11**, 281–296

Received 7 November 2003/24 November 2003; accepted 26 November 2003
Published as BJ Immediate Publication 26 November 2003, DOI 10.1042/BJ20031706